 CMES, vol.56, no.2, pp.113-130, 2010

Effect of Patch Mechanical Properties on Right Ventricle Function Using MRI-Based Two-Layer Anisotropic Models of Human Right and Left Ventricles

Dalin Tang[1], Chun Yang[1,2], Tal Geva[3]
Glenn Gaudette[4] and Pedro J. del Nido[5]

Abstract: Right and left ventricle (RV/LV) combination models with three different patch materials (Dacron scaffold, treated pericardium, and contracting myocardium), two-layer construction, fiber orientation, and active anisotropic material properties were introduced to evaluate the effects of patch materials on RV function. A material-stiffening approach was used to model active heart contraction. Cardiac magnetic resonance (CMR) imaging was performed to acquire patient-specific ventricular geometries and cardiac motion from a patient with severe RV dilatation due to pulmonary regurgitation needing RV remodeling and pulmonary valve replacement operation. Computational models were constructed and solved to obtain RV stroke volume, ejection fraction, patch area variations, and stress/strain data for patch comparisons. Our results indicate that the patch model with contracting myocardium leads to decreased stress level in the patch area, improved RV function and patch area contractility. Maximum Stress-P_1 (maximum principal stress) value at the center of the patch from the Dacron scaffold patch model was 350% higher than that from the other two models. Patch area reduction ratio was 0.3%, 3.1% and 27.4% for Dacron scaffold, pericardium, and contracting myocardium patches, respectively. These findings suggest that the contracting myocardium patch model may lead to improved recovery of RV function in patients with severe chronic pulmonary regurgitation.

Keywords: right ventricle, congenital heart disease, heart model, Dacron scaf-

[1] Corresponding author, dtang@wpi.edu, Worcester Polytechnic Institute, MA 01609, USA
[2] School of Mathematical Sciences, Beijing Normal University, Laboratory of Mathematics and Complex Systems, Ministry of Education, Beijing, China
[3] Department of Cardiology, Children's Hospital, Boston, Department of Pediatrics, Harvard Medical School Boston, MA 02115 USA
[4] Department of Biomedical Engineering, Worcester Polytechnic Institute, MA 01609, USA
[5] Dept. of Cardiac Surgery, Children's Hospital, Boston, Department of Surgery, Harvard Medical School, Boston, MA 02115 USA

fold patch.

1 Introduction

Right ventricular (RV) dysfunction is a common cause of heart failure in patients with congenital heart defects and often leads to impaired functional capacity and premature death [del Nido, 2006]. Patients with repaired Tetralogy of Fallot (ToF), a congenital heart defect which includes a ventricular septal defect and severe right ventricular outflow obstruction, account for the majority of cases with late onset RV failure. The current surgical approach, which includes pulmonary valve replacement/insertion (PVR), has yielded mixed results [Therrien, Siu, and McLaughlin, (2000); Vliegen et al., (2002); Waien et al. (1992)]. One reason for the unpredictable results is the fact that the PVR surgery only addresses pulmonary regurgitation. New surgical options including scar tissue reduction and RV remodeling have been proposed in order to improve RV function recovery [del Nido, (2006)]. Various RV reconstruction techniques are being investigated, including patch designs (patch materials, sizes, and shapes) and in the laboratory, myocardial tissue regeneration techniques are being developed for the potential that viable myocardium may be regenerated or placed in the patch area [Kochupura and Gaudette et al., (2005); Kelly and Gaudette et al., (2009)]. Wald and Geva et al. (2009) investigated effects of regional dysfunction on global RV function in patients with repaired ToF and reported that localized dysfunction in the region of the RV outflow tract patch adversely affects global RV function and regional measures, and may have important implications for patient management. Recent advances in computational modeling, methods and computer technology have made it possible for computer-simulated procedures (virtual surgery) to be used in clinical decision-making process to replace empirical and often risky clinical experimentation to examine the efficiency and suitability of various reconstructive procedures and patch design in diseased hearts [McCulloch (2007); McCulloch, Waldman, Rogers, Guccione (1992); Bloomgarden, Fayad and Axel et al. (1997); Guccione, Costa, McCulloch (1995); Guccione, Le Prell, de Tombe, Hunter, (1997); Guccione, McCulloch, (1993); Guccione, Waldman, McCulloch (1993); Hunter, Pullan, Smaill (2003); Nash and Hunter (2000); Saber et al. (2001); Tang, Yang, Geva, and del Nido (2007,2008); Vetter and McCulloch (2000); Ghista et al., (2005)].

In this paper, cardiac magnetic resonance (CMR) imaging-based two-layer active anisotropic models of human right and left ventricles (RV/LV) were constructed to investigate the effects of patch mechanical properties on RV size and function. Active ventricular contraction was modeled by a material stiffening approach. Three patch materials were considered: Patch 1 - Dacron scaffold; Patch 2 - pericardium, usually from the patient, treated with gluteraldehyde to crosslink the collagen and

making it stiffer; Patch 3 – viable contracting myocardium (not currently available but represents future direction). The 3D CMR-based RV/LV/Patch combination models were solved to obtain 3D ventricular deformation and stress/strain distributions for accurate assessment of RV mechanical conditions and function. The computational models were validated by CMR data and then used to assess the effect of patch material properties with the ultimate goal of improving recovery of RV function after surgery.

The RV/LV/Patch model has complex geometries and multi-physics interactions and requires sophisticated numerical methods to solve it. There have been considerable advances in development of unstructured finite element methods and various meshless methods, capable of handling a wide range of engineering applications [Atluri (2004); Atluri et al. (2004, 2006a, 2006b); Bathe (2002); Ahrem, Beckert and Wendland (2006); Han et al. (2004a, 2004b, 2005, 2006, 2007]. A series of meshless local Petrov-Galerkin (MLPG) methods were introduced to solved 3-dimensional elasto-static and dynamical problems [Han and Atluti (2004a, 2004b, 2007); Han, Liu, Rajendran, Atluri (2006)] and nonlinear problems with large deformation and rotations [Han, Rajendran and Atluri (2004)]. Li and Atluri developed the MLPG mixed collocation method for material orientation and topology optimization [Li and Atluri, (2008)]. A "mixed" approach was introduced to improve the MLPG method using finite volume method [Atluri, Han and Rajendran (2004)] and finite difference method [Atluri, Liu, and Han, (2006a, 2006b); Hu, Young, Fan (2008)]. Wang and Wang investigated structural shape and topology optimization using an implicit free boundary parameterization method [Wang and Wang, (2006)]. Sladek et al. applied the MLPG method to models of intelligent material systems, 3D anisotropic functionally graded solids, and deformable shells [Sladek, Sladek, Solek, and Atluri, (2008); Sladek, Sladek, Tan,and Atluri, (2008)]. Cai and Zhu introduced a local meshless Shepard and least square interpolation method based on local weak form [Cai and Zhu, 2008]. A new meshless interpolation scheme for MLPG method was developed by Ma [Ma (2008)]. Zheng et al. introduced a finite volume meshless local Petrov-Galerkin method for topology optimization design of the continuum structures was introduced by Zheng et al. (2009). Analysis of structure with material interfaces was performed by Masuda and Noguchi [Masuda, Noguchi (2006)]. Perko and Sarler studied weight function shape parameter optimization in meshless methods for non-uniform grids [Perko and Sarler (2007)]. A meshless local natural neighbour interpolation method was applied to structural dynamic analysis by Liu et al. [Liu, Chen, Li, and Cen, 2008]. Numerical methods were also developed to solve problems with free and moving boundaries [Zohouri, Pirooz, and Esmaeily (2005)]. Ma, Lu and Komanduri studied structured mesh refinement in generalized interpolation material point

(GIMP) method for simulation of dynamic problems [Ma, Lu, and Komanduri, (2006)]. Zhang et al. developed high-fidelity tetrahedral mesh generation techniques for models based on medical imaging data with fluid-structure interactions [Zhang et al., (2009)]. Young et al. developed hypersingular meshless method for solving 3D potential problems with arbitrary domain [Young et al. (2009)]. Yang et al. used unstructured finite element method to solve MRI-based vulnerable plaque models with fluid-structure interactions [Yang et al., 2007, 2008]. Regularized meshless method for irregular domain problems was investigated by Song and Chen [Song and Chen, (2009)]. Sellountos, Sequeira and Polyzos performed elastic transient analysis with MLPG(LBIE) method and local RBFs [Sellountos, Sequeira and Polyzos, (2009)]. Lucas et al. proposed an automated approach for mesh adaptation to enhance accuracy of algorithms [Lucas, van Zuijlen and Bijl, (2009)]. A boundary element formulation for incremental nonlinear elastic deformation of compressible solids was proposed by Colli, Gei and Bigoni [Colli, Gei and Bigoni, (2009)]. In this paper, a geometry-fitting mesh generation method was developed to construct the two-layer RV/LV/Patch model with patient-specific ventricle geometries. Details are given below.

2 Data Acquisition, Models and Methods

2.1 Data acquisition

Cardiac MRI (CMR) studies were performed by Dr. Tal Geva to acquire patient-specific ventricular geometry for patients needing RV remodeling and pulmonary valve replacement operations before and after scheduled surgeries. The RV and LV were imaged using ECG-gated, breath-hold steady state free precession cine MR in the ventricular short axis (12-14 equidistant slices covering the ventricles from base to apex; slice thickness 6-8 mm; interslice gap 0-2 mm; 30 frames per cardiac cylcle). Valve and patch positions were determined with cine MR imaging, flow data, and delayed enhancement CMR to delineate location and extent of scar/patch. The CMR findings were subsequently confirmed by the intra-operative observations (del Nido). Three dimensional RV/LV geometry and computational mesh were constructed following the procedures described in [Tang, Yang, Geva, and del Nido (2007, 2008)]. Fig. 1 shows one set of pre-operation CMR images from a patient with repaired TOF and severe RV dilatation. The figure depicts segmented contours for both tissue and scaffold patches. Fig. 2 shows the stacked contours, RV/LV inner/outer surfaces, valve and patch positions, two-layer fiber orientations, and a cut surface showing different patch thicknesses.

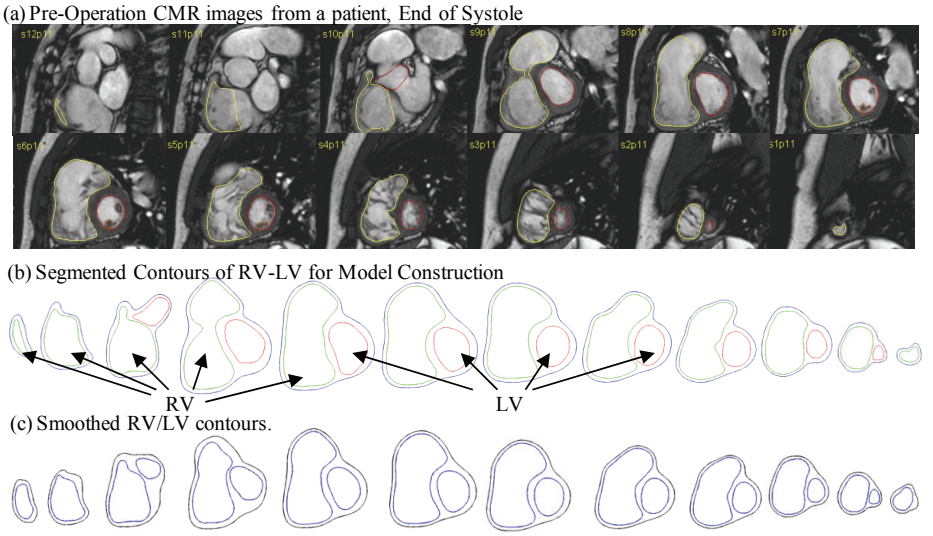

Figure 1: Pre-operative MR images (end-systole) acquired from a patient, segmented RV/LV contours, and smoothed contours for 3D model construction.

2.2 The passive and active anisotropic models, two-layer model construction

The RV and LV materials were assumed to be hyperelastic, anisotropic, nearly-incompressible and homogeneous. Scar tissue and patch material (other than Patch 3) were assumed to be hyperelastic, isotropic, nearly-incompressible and homogeneous. The governing equations for the structure models are:

$$\rho v_{i,tt} = \sigma_{ij,j}, \quad i,j = 1,2,3; \text{ sum over } j, \tag{1}$$

$$\varepsilon_{ij} = (v_{i,j} + v_{j,i} + v_{\alpha,i} v_{\alpha,j})/2, \quad i,j,\alpha = 1,2,3, \tag{2}$$

where σ is the stress tensor, ε is the strain tensor, $\mathbf{v}$ is displacement, $\mathrm{f}_{,j}$ stands for derivative of f with respect to the jth variable, and ρ is material density. Equations (1)-(2) were used for RV/LV muscle, patch, and scar tissue. The normal stress was assumed to be zero on the outer surface and to be equal to the pressure specified inside the ventricles (Fig. 3) [Berne, Levy, Koeppen, Stanton (2004)],

$$p|_{RV} = p_{RV}(t), \quad p|_{LV} = p_{LV}(t), \tag{3}$$

The nonlinear Mooney-Rivlin model was used to describe the nonlinear anisotropic and isotropic material properties of the material with parameter values chosen to

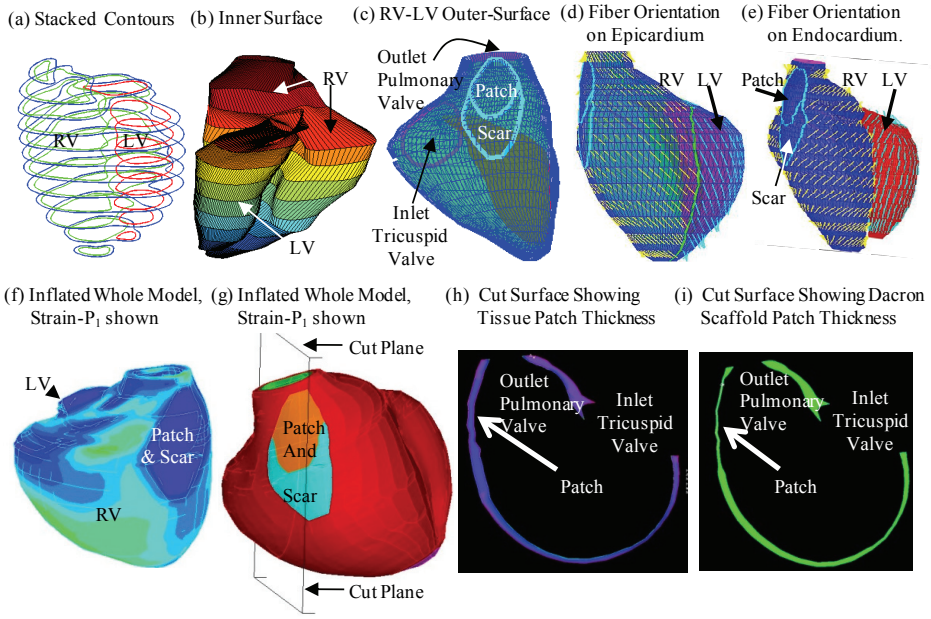

Figure 2: Re-constructed 3D geometry of RV and LV showing inner and outer surfaces, valve, and patch positions, two-layer fiber orientation, and patch thickness.

match experimental data available and adjusted to reflect stiffness variation of different materials [Humphrey (2002); McCulloch (2007); Sacks and Chuong (1993)]. The strain energy function for the isotropic modified Mooney-Rivlin model is given by [Bathe (2002); Yang, Tang, Haber, Geva, del Nido (2007)]:

$$W = c_1(I_1 - 3) + c_2(I_2 - 3) + D_1[exp(D_2(I_1 - 3)) - 1], \tag{4}$$

where I_1 and I_2 are the first and second strain invariants given by,

$$I_1 = \sum C_{ii}, \quad I_2 = 1/2[I_1^2 - C_{ij}C_{ij}], \tag{5}$$

$C = [C_{ij}] = X^T X$ is the right Cauchy-Green deformation tensor, $X = [X_{ij}] = [\partial x_i / \partial a_j]$, (x_i) is current position, (a_i) is original position, c_i and D_i are material parameters chosen to match experimental measurements [Humphrey (2002); McCulloch (2007); Sacks and Chuong (1993)]. The strain energy function for the anisotropic modified Mooney-Rivlin model anisotropic model was obtained by adding an additional anisotropic term in Eq. (3) [Bathe (2002); Holzapfel, Gasser, Ogden (2000)]:

$$W = c_1(I_1 - 3) + c_2(I_2 - 3) + D_1[\exp(D_2(I_1 - 3)) - 1], \tag{6}$$

where = c_{ij} $(\mathbf{n}_f)_i$ $(\mathbf{n}_f)_j$, c_{ij} is the Cauchy-Green deformation tensor, $\mathbf{n}_f$ is the fiber direction, K_1 and K_2 are material constants [Bathe (2002)]. Choosing c_1=0.351 KPa, c_2=0, D_1=0.0633 KPa, D_2 =5.3, K_1=1.913 KPa, K_2 =6.00, it was shown [Tang, Yang, Geva, del Nido, (2007)] that our model agrees very well with the model given in [McCulloch et al. (1992, 2007)]. Scar tissue and treated pericardium were assumed to be 10 and 20 times stiffer than that of the normal RV tissue, respectively. Stress-stretch curves of normal myocardium, scar, and treated pericardium are given in Fig. 3. The Young's modulus for the Dacron scaffold patch was measured to be 80 MPa.

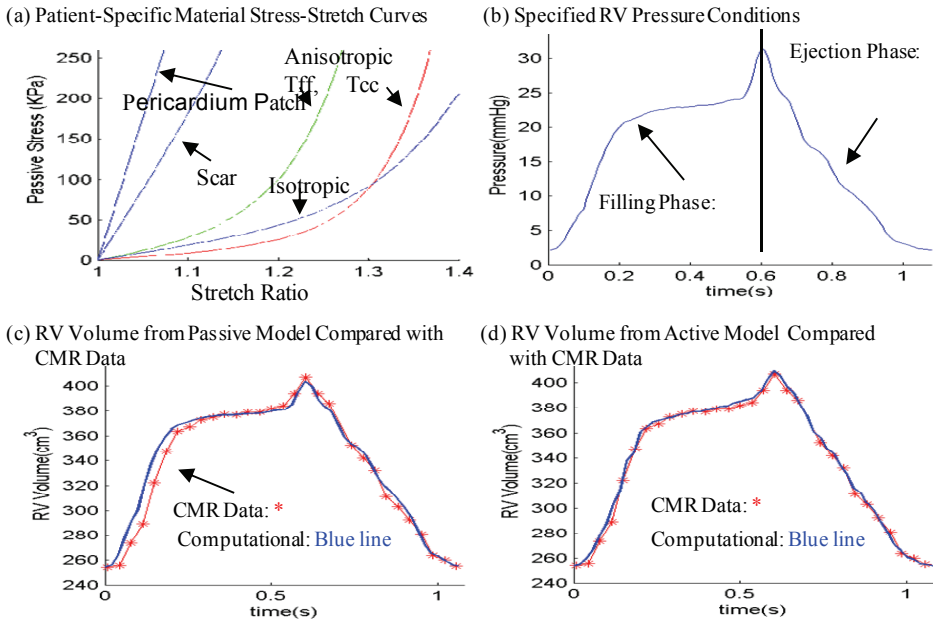

Figure 3: Patient-specific material stress-stretch curves for ventricular tissue, scar and patch materials, specified pressure conditions, and computed RV volumes compared with CMR recorded data showing good agreement (CMR min=254.5 ml, max=406.9 ml; active model predictions: Min= 254.3 ml, Max= 409.2 ml; error margin <1%). The active model has better agreement with CMR data because the active tension term was adjusted for every time step to match with CMR volume data. Tff is the stress in fiber direction. Tcc is the stress in fiber circumferential direction.

Modeling active heart contraction is much harder because stress in a pumping human heart cannot be measured in vivo non-invasively (at least not with available

technology in current practice). Since it is very hard to separate and measure the passive and active stresses/strains in clinical practice, we chose to specify time-dependent material stiffness parameters to model RV tissue stiffening and active RV contraction. RV muscle fibers will contract/relax by following a time-dependent stiffening/relaxation material model. The time-dependent material parameters in (4)-(6) (all parameters were functions of time) were numerically determined to match CMR measured RV volume curves (see Fig. 3).

As patient-specific fiber orientation data is not available in current practice, we chose to construct a two-layer RV/LV model and set fiber orientation angles using fiber angles given in Hunter [Hunter, Pullan, Smaill, (2003)] (also see Fig. 4). Fiber orientation can be adjusted when patient-specific data becomes available.

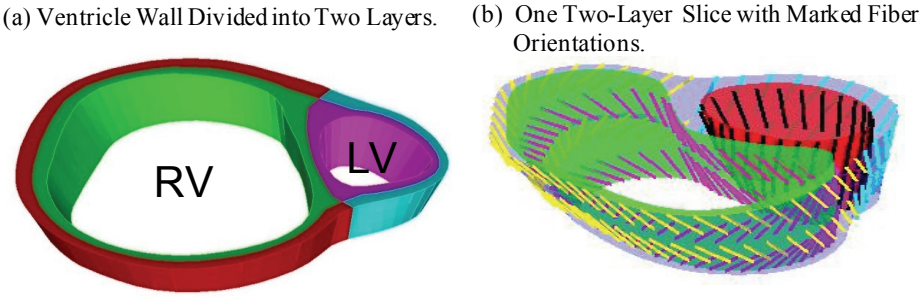

Figure 4: Two-layer model construction with fiber orientations

2.3 Solution methods and simulation procedures

Equations (1)-(6) give the RV/LV/Patch model which was solved by ADINA (ADINA R&D, Watertown, MA, USA) using unstructured finite elements and the Newton-Raphson iteration method [Bathe (2002)]. The "Re-Start" feature in ADINA was used to adjust material parameters at each numerical step for the active models. While our stiffening material mechanism is different from that for a real actively-contracting heart, our simulated RV motion and volume change can provide results matching patient-specific volume data with properly-adjusted material parameters.

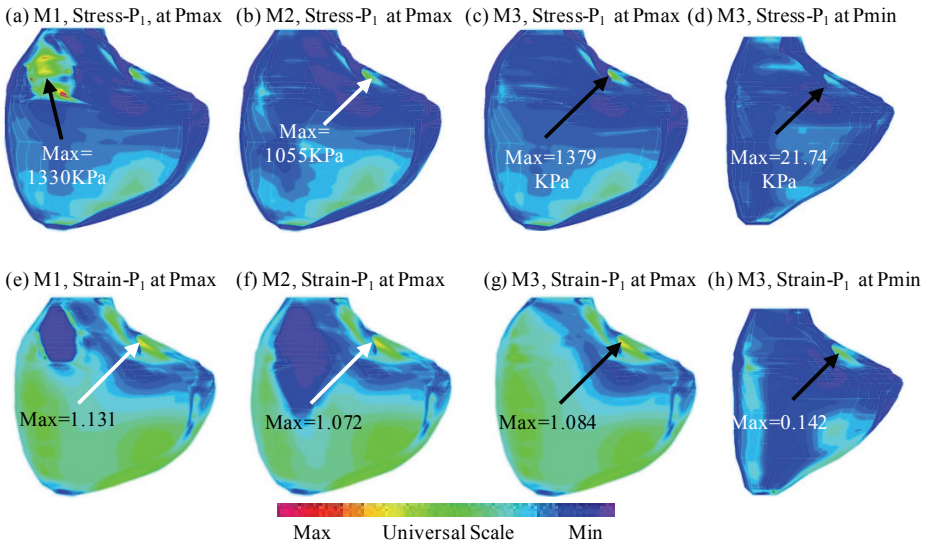

Figure 5: Stress and strain distributions on the inner RV surface from the three patch models showing Dacron scaffold patch model has non-uniform stress/strain distributions.

3 Results

3.1 Comparison of stress/strain behaviors of the three patch models

The RV/LV/Patch models with passive and active material properties used for the normal RV tissues were validated by using CMR-measured RV volume curves throughout the cardiac cycle (see Fig. 3). Simulations were conducted using three models: Model 1 (M1) consisted of Dacron scaffold patch; Model 2 (M2) consisted of glutaraldehyde-treated pericardial patch; and Model 3 (M3) consisted of viable contracting myocardium in the patch area. Fig. 5 presents maps (band plots) of maximum principal stress (Stress-P_1) and strain (Strain-P_1) from the three models to give an overall view of the stress/strain distributions. As expected, Dacron scaffold patch gave higher stress concentration and low strain. To obtain more specific information caused by the patch differences, 5 locations (X1-X5) were selected and Fig. 6 shows Stress-P_1 tracked at those five locations over a cardiac cycle. Stress-P_1 at X5 from the Dacron scaffold patch was 314.2 kPa, which is about 350% higher than that (70.3 kPa) from M2 and M3 (68.9kPa). M3 (viable myocardium) showed the lowest overall stress level in the patch area.

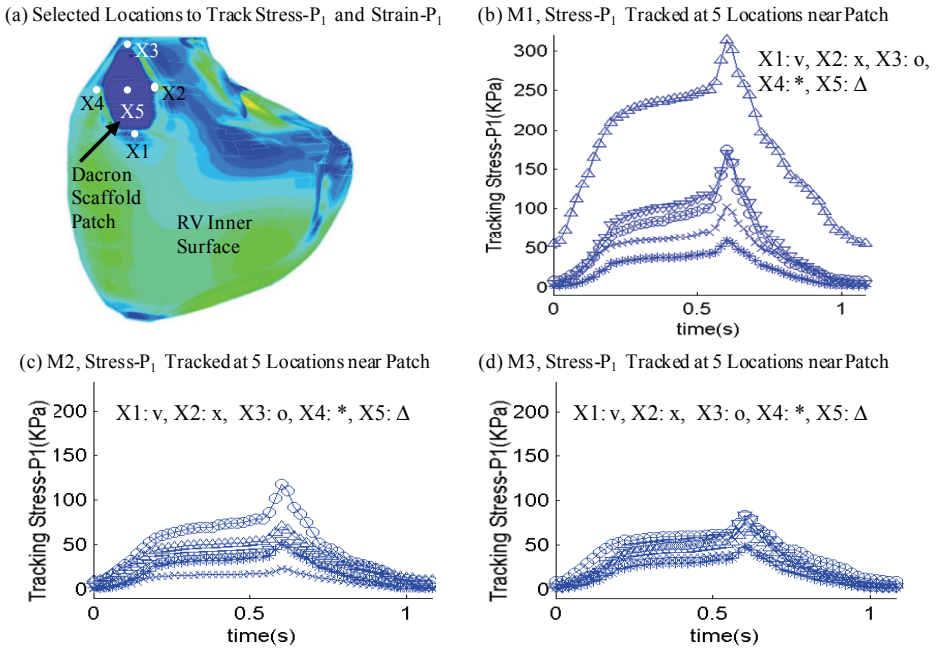

Figure 6: Stress-P_1 variations tracked at selected tracking locations for the three patch models show that stress/strain levels (around the patches) are considerably lower from Patch Model 3 than that from the other two models. Lower stress levels may indicate that the ventricle operates under more favorable mechanical conditions.

3.2 Assessment of RV cardiac function and regional patch area changes

Results from the three patch models were used to evaluate their effect on RV function. The two measures of RV function evaluated were stroke volume (SV) and ejection fraction (EF) defined as:

SV = RV End Diastolic Volume (RVEDV) – RV End Systolic Volume (RVESV); (7)

EF = [RVEDV - RVESV]/RVEDV, (8)

RVEDV, RVESV, SV and EF values for M1, M2, and M3 are summarized in Table 1. The results indicate that Patch Model 3 (M3) would provide about 8% improvement in EF, compared to Patch Model 1 (Dacron scaffold). The observation that EF values for M1 and M2 were very close can be attributed to the fact that both patch

materials are considerably stiffer than normal myocardium and that the total patch area is only a small portion of the total RV surface area.

To concentrate on the patch area and illustrate the differences among the three patch materials, patch area changes are summarized in Table 2 where

RVEDPA= RV End Diastolic Patch Area, (9)

RVESPA= RV End Systolic Patch Area. (10)

Patch 3 had an impressive 27.4% patch fractional area change, a regional tissue contracting measure similar to ejection fraction for the whole ventricle. Dacron patch area hardly changed (fractional area change was only 0.3%) because the scaffold material was very stiff. Fig. 7 shows the area variations of the three patches over the cardiac cycle.

Table 1: Stroke volume and ejection fraction comparisons for three patch models showing regenerated myocardium model has the best ejection fraction.

Cases	Patch Model 1 Dacron Scaffold	Patch Model 2 pericardium	Patch Model 3 Myocardium
RVEDV (ml)	408.4	409.2	427.1
RVESV (ml)	257.0	254.3	255.4
SV (ml)	151.4	154.9	171.8
Ejection Fraction (%)	37.1%	37.9%	40.2%

Table 2: Patch area change comparisons for three patch models showing regenerated myocardium model has the best patch area change ratio.

Cases	Patch Model 1 Dacron Scaffold	Patch Model 2 pericardium	Patch Model 3 Myocardium
RVEDPA (cm2)	8.148	8.025	10.830
RVESPA (cm2)	8.127	7.772	7.862
Patch Area Change	0.021	0.253	2.968
Patch Area Change Fraction (%)	0.3%	3.1%	27.4%

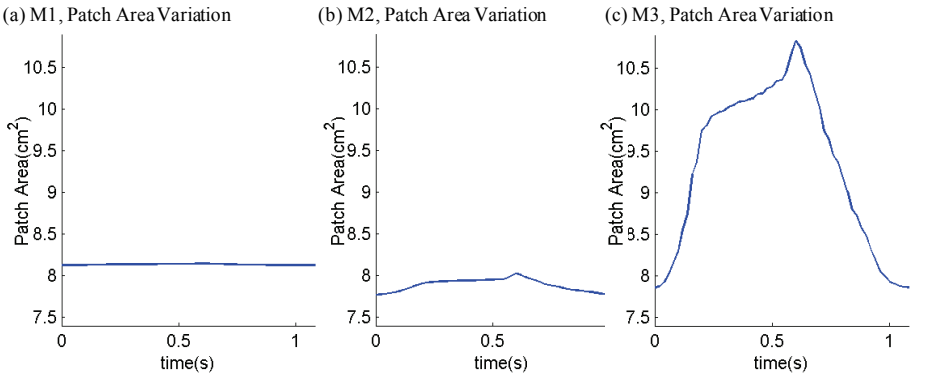

Figure 7: Patch area variations showing that patch with contracting myocardium material provided larger patch area variations which led to better ventricular ejection fraction. Patch 1 had a larger starting area because the patch was very thin and was at the outer surface of the right ventricle.

4 Discussion

4.1 Motivation to develop myocardium tissue regeneration techniques

With the rapidly increasing number of late survivors of tetralogy of Fallot repair, surgical management of patients with right ventricular dysfunction has become a major clinical challenge. The wide variability in clinical status, extent of right ventricular dilatation, scarring, and dysfunction at the time of presentation has resulted in disparate surgical results with pulmonary valve insertion alone [Waien et al. (1992)]. Del Nido and Geva et al. have proposed aggressive scar tissue trimming and RV volume remodeling as a way to improve RV function after pulmonary valve replacement surgery. Clearly, contracting myocardium would be the most desirable patch material for RV remodeling, likely leading to recovery of ventricular functions after PVR and RV remodeling surgery. Results presented in this paper indicate that tissue regeneration techniques that restore RV myocardium have the potential to improve ventricular function.. Computational simulations may be used to supplement/replace empirical and often risky clinical experimentation, or even guide the design of new clinical trials to examine the efficiency and suitability of various reconstructive procedures in diseased hearts so that optimal design can be found.

4.2 Model limitations

Several improvements can be added to our models in the future for better accuracy and applicability: a) fluid-structure interactions can be added to obtain blood flow shear stress and investigate its influence on myocardial regeneration and RV remodeling; b) direct measurements of tissue mechanical properties will be very desirable for improved accuracy of our models; c) inclusion of pulmonary valve mechanics in the model; d) multi-scale models including organ, cell, and gene investigations; and e) active contraction model. Another way to add active contraction into our model is to introduce an external force field which is tied to fiber structure and orientations. The difficulty is that measurement and validation of the external force field are not currently available. Information obtained from animal models could be used as an approximate starting point [Guccione et al. (1995, 1997)].

5 Conclusion

Our preliminary results indicate that a patch model using viable myocardium leads to decreased stress level in the patch area, improved right ventricular function, and higher patch area contractility. Maximum Stress-P_1 value at the center of the patch from the Dacron scaffold patch model was 305% higher than that from the other two models. Patch area reduction ratio was 0.3%, 3.1% and 27.4% from Dacron scaffold patch, treated pericardium patch, and viable contracting myocardial patch, respectively. The techniques to regenerate myocardium combined with other surgical procedures have promising potential to improve ventricular function in patients with repaired TOF and other congenital heart disease.

Acknowledgement: This research was supported in part by NIH-1R01-HL 089269 (del Nido, Tang, Geva), NIH-HL63095 (PI: del Nido) and NIH-NHLBI 5P50HL074734 (PI: Geva; Co-Investigator: del Nido). Professor Yang was also supported in part by priority discipline of Beijing Normal University.

References

Ahrem, R.; Beckert, A.; Wendland, H. (2006): A meshless spatial coupling scheme for large-scale fluid-structure-interaction problems, *CMES: Computer Modeling in Engineering & Sciences,* 12(2):121-136.

Atluri, S. N. (2004): The Meshless local-Petrov-Galerkin method for domain & BIE discretizations, Tech Science Press, Forsyth, GA.

Atluri, S. N.; Han, Z. D.; Rajendran, A. M. (2004): A new implementation of the meshless finite volume method, through the MLPG "mixed" approach, *CMES:*

Computer Modeling in Engineering & Sciences, 6(6):491-513.

Atluri, S. N.; Liu, H. T.; Han, Z. D. (2006a): Meshless local Petrov-Galerkin (MLPG) mixed collocation method for elasticity problems, *CMES: Computer Modeling in Engineering & Sciences,* 14(3):141-152.

Atluri, S. N.; Liu, H. T.; Han, Z. D. (2006b): Meshless local Petrov-Galerkin (MLPG) mixed finite difference method for solid mechanics, *CMES: Computer Modeling in Engineering & Sciences,* 15(1):1-16.

Bathe, K. J., Eds, (2002): *Theory and Modeling Guide,* Vol I & II: ADINA and ADINA-F, ADINA R & D, Inc., Watertown, MA, USA.

Berne, R.M.; Levy, M.N.; Koeppen, B.M.; Stanton, B.A. (2004), *Physiology,* Fifth Edition, Mosby, Elsevier, St. Louis, MO.

Bloomgarden, D. C.; Fayad, Z. A.; Ferrari, V. A.; Chin, B.; Sutton, M. G.; and Axel, L. (1997): Global Cardiac Function Using Fast Breath-Hold MRI: Validation of New Acquisition and Analysis Techniques, *Magn Reson Med.* 37, 683-692.

Cai, Y.C.; Zhu, H. H. (2008): A local meshless Shepard and least square interpolation method based on local weak form, *CMES: Computer Modeling in Engineering & Sciences,* 34(2):179-204.

Colli, S.; Gei, M.; Bigoni, D. (2009): A boundary element formulation for incremental nonlinear elastic deformation of compressible solids, *CMES: Computer Modeling in Engineering & Sciences,* 40(1):29-62.

del Nido, P. J. (2006): Surgical Management of Right Ventricular Dysfunction Late after Repair of Tetralogy of Fallot: Right Ventricular Remodeling Surgery, *Semin Thorac Cardiovasc Surg Pediatr Card Surg Annu.* 29-34.

Ghista, D. N.; Zhong, L.; Chua, L. P.; Ng, E. Y-K.; Lim, S. T.; Tan, R. S.; Chua, T. S-J. (2005): Systolic Modeling of the Left Ventricle as a Mechatronic System: Determination of Myocardial Fiber's Sarcomere Contractile Characteristics and New Performance Indices, *MCB: Molecular & Cellular Biomechanics,* 2(4), 217-234.

Guccione, J. M.; Costa, K. D.; McCulloch, A. D. (1995): Finite element stress analysis of left ventricular mechanics in the beating dog heart, *J Biomech.* 28(10), 1167-77.

Guccione, J. M.; Le Prell, G. S.; de Tombe, P. P.; Hunter, W. C. (1997): Measurements of active myocardial tension under a wide range of physiological loading conditions, *J Biomech.* 30(2), 189-192.

Guccione, J. M.; McCulloch, A. D. (1993): Mechanics of active contraction in cardiac muscle: Part I–Constitutive relations for fiber stress that describe deactivation, *J Biomech Eng.* 115(1), 72-81.

Guccione, J. M.; Waldman, L. K.; McCulloch, A. D. (1993): Mechanics of active contraction in cardiac muscle: Part II-Cylindrical models of the systolic left ventricle, *J Biomech Eng.* 115(1), 82-90.

Han, Z. D.; Atluri, S. N. (2004a): Meshless local Petrov-Galerkin (MLPG) approaches for solving 3D problems in elasto-statics, *CMES: Computer Modeling in Engineering & Sciences*, 6(2): 169-188.

Han, Z.D.; Atluri S. N. (2004b): A meshless local Petrov-Galerkin (MLPG) approach for 3-dimensional elasto-dynamics, *CMC: Computers, Materials & Continua*, 1(2):129-140.

Han, Z. D.; Atluri, S. N. (2007): A systematic approach for the development of weakly-singular BIEs , *CMES: Computer Modeling in Engineering & Sciences,* 21(1):41-52.

Han, Z. D.; Liu, H. T.; Rajendran, A. H.; Atluri, S. N. (2006): The applications of meshless local Petrov-Galerkin (MLPG) approaches in high-speed impact, penetration and perforation problems, *CMES: Computer Modeling in Engineering & Sciences,* 14(2):119-128.

Han, Z. D.; Rajendran, A. M.; Atluri, S. N. (2005): Meshless local Petrov-Galerkin (MLPG) approaches for solving nonlinear problems with large deformations and rotations, *CMES: Computer Modeling in Engineering & Sciences,* 10(1):1-12.

Holzapfel, G. A.; Gasser, T. C.; Ogden, R. W. (2000): A new constitutive framework for arterial wall mechanics and a comparative study of matereial models, *Journal of Elasticity*, 61, 1-48.

Hu, S. P.; Young, D. L.; Fan, C. M. (2008): FDMFS for diffusion equation with unsteady forcing function, *CMES: Computer Modeling in Engineering & Sciences,* 24(1):1-20.

Humphrey, J. D. (2002): *Cardiovascular Solid Mechanics*, Springer-Verlag, New York.

Hunter, P. J.; Pullan, A. J.; Smaill, B. H. (2003): Modeling Total Heart Function, *Annu Rev Biomed Eng*., 5, 147-77.

Kelly, D. J.; Rosen, A. B.; Schuldt, A. J.; Kochupura, P. V.; Doronin, S. V.; Potapova, I. A.; Azeloglu, E. U.; Badylak, S. F.; Brink, P. R.; Cohen, I. S.; Gaudette, G. R. (2009): Increased myocyte content and mechanical function within a tissue-engineered myocardial patch following implantation. *Tissue Eng Part A.* 15(8):2189-2201.

Kochupura, P. V.; Azeloglu, E. U.; Kelly, D. J.; Doronin, S. V.; Badylak, S. F.; Krukenkamp, I. B.; Cohen, I. S.; Gaudette, G. R. (2005): Tissue-engineered

myocardial patch derived from extracellular matrix provides regional mechanical function. *Circulation,* 30;112(9 Suppl):I144-9.

Li, S. and Atluri, S. N. (2008): The MLPG mixed collocation method for material orientation and topology optimization of anisotropic solids and structures, *CMES: Computer Modeling in Engineering & Sciences,* 30(1):37-56.

Liu, Y. H.; Chen, S. S.; Li, J.; and Cen, Z. Z. (2008): A meshless local natural neighbor interpolation method applied to structural dynamic analysis, *CMES: Computer Modeling in Engineering & Sciences,* 31(3):145-156.

Lucas, P.; van Zuijlen, A. H.; Bijl, H. (2009): An automated approach for solution based mesh adaptation to enhance numerical accuracy for a given number of grid cells applied to steady flow on hexahedral grids, *CMES: Computer Modeling in Engineering & Sciences,* 41(2):147-176.

Ma, J.; Lu, H.; Komanduri, R. (2006): Structured mesh refinement in generalized interpolation material point (GIMP) method for simulation of dynamic problems, *CMES: Computer Modeling in Engineering & Sciences,* 12(3):213-228

Ma, Q. W. (2008): A new meshless interpolation scheme for MLPG_R method, *CMES: Computer Modeling in Engineering & Sciences,* 23(2):75-90.

Masuda, S; Noguchi, H. (2006): Analysis of structure with material interface by meshfree method, *CMES: Computer Modeling in Engineering & Sciences,* 11(3):131-144.

McCulloch, A. M. et al., (2007): Continuity 6 (a package distributed free by the National Biomedical Computation Resource), www.continuity.ucsd.edu.

McCulloch, A. M.; Waldman, L.; Rogers, J.; Guccione, J. (1992): Large-scale finite element analysis of the beating heart, *Critical Rev. in Biomedical Engineering*, 20(5,6): 427-449.

Nash, M. P.; Hunter, P. J. (2000): Computational Mechanics of the Heart, From Tissue Structure to Ventricular Function, *Journal of Elasticity*, 61:113-141.

Perko, J.; Sarler, B. (2007): Weight function shape parameter optimization in meshless methods for non-uniform grids, *CMES: Computer Modeling in Engineering & Sciences,* 19(1):55-68.

Saber, N. R.; Gosman, A. D.; Wood, N. B.; Kilner, P. J.; Charrier, C. L.; Firman, D. N. (2001): Computational Flow Modeling of the Left Ventricle Based on In Vivo MRI Data: Initial Experience, *Annals of Biomech. Engng.,* 29, 275-283.

Sacks, M. S.; Chuong, C. J., (1993): Biaxial Mechanical Properties of Passive Right Ventricular Free Wall Myocardium, *J Biomech Eng*, 115:202-205.

Sellountos, E. J.; Sequeira, A.; Polyzos, D. (2009): Elastic transient analysis with MLPG(LBIE) method and local RBFs, *CMES: Computer Modeling in Engineering*

& Sciences, 41(3):215-242.

Sladek, J.; Sladek, V.; Solek, P.; Atluri, S.N. (2008): Modeling of intelligent material systems by the MLPG, *CMES: Computer Modeling in Engineering & Sciences,* 34(3):273-300.

Sladek, J.; Sladek, V.; Tan, C. L.; Atluri, S.N. (2008): Analysis of transient heat conduction in 3D anisotropic functionally graded solids, by the MLPG method, *CMES: Computer Modeling in Engineering & Sciences,* 32(3):161-174.

Sladek, J.; Sladek, V.; Wen, P. H.; Aliabadi, M.H. (2006): Meshless local Petrov-Galerkin (MLPG) method for shear deformable shells analysis, *CMES: Computer Modeling in Engineering & Sciences,* 13(2):103-118

Song, R. and Chen, W. (2009): An investigation on the regularized meshless method for irregular domain problems, *CMES: Computer Modeling in Engineering & Sciences,* 42(1):59-70.

Tang, D.; Yang, C.; Geva, T.; del Nido, P. J. (2008): Patient-Specific MRI-Based 3D FSI RV/LV/Patch Models for Pulmonary Valve Replacement Surgery and Patch Optimization, *J. of Biomech. Engineering*, 130(4)041010.

Tang, D.; Yang, C.; Geva, T.; del Nido, P. J. (2007): Two-Layer Passive/Active Anisotropic FSI Models with Fiber Orientation: MRI-Based Patient-Specific Modeling of Right Ventricular Response to Pulmonary Valve Insertion Surgery, *MCB: Molecular & Cellular Biomechanics*, 4(3):159-176.

Therrien, J.; Siu, S. C.; McLaughlin, P. R. (2000): Pulmonary Valve Replacement in Adults Late after Repair of Tetralogy of Fallot: Are We Operating too Late? *J Am Coll Cardiol.* 36:1670-5.

Vetter, F. J.; McCulloch, A. D. (2000): Three-Dimensional Stress and Strain in Passive Rabbit Left Ventricle: A Model Study, *Annals of Biomed. Engng*. 28:781-792.

Vliegen, H. W.; Van Straten, A.; De Roos, A.; Roest, A. A.; Schoof, P. H.; Zwinderman, A. H.; Ottenkamp, J.; Van Der Wall, E. E.; Hazekamp, M. G. (2002): Magnetic Resonance Imaging to Assess the Hemodynamic Effects of Pulmonary Valve Replacement in Adults Late after Repair of Tetralogy of Fallot, *Circulation,* 106:1703-1707.

Waien, S.A.; Liu, P. P.; Ross, B. L.; Williams, W. G.; Webb, G. D.; McLaughlin, P. R. (1992): Serial follow-up of adults with repaired tetralogy of Fallot. *J Am Coll Cardiol.* 20, 295-300.

Wald, R. M.; Haber, I.; Wald, R.; Valente, A. M.; Powell, A. J.; Geva, T. (2009): Effects of Regional Dysfunction and Late Gadolinium Enhancement on Global Right Ventricular Function and Exercise Capacity in Patients with Repaired

Tetralogy of Fallot, *Circulation*. 119:1370-1377.

Wang, S.Y.; Wang, M.Y. (2006): Structural shape and topology optimization using an implicit free boundary parameterization method, *CMES: Computer Modeling in Engineering & Sciences,* 13(2):119-148.

Yang, C.; Tang, D.; Haber, I.; Geva, T.; del Nido, P. J., (2007): In Vivo MRI-Based 3D FSI RV/LV Models for Human Right Ventricle and Patch Design for Potential Computer-Aided Surgery Optimization, *Computers & Structures*, 85, 988-997.

Yang, C.; Tang, D.; Yuan, C.; Hatsukami, T. S.; Zheng, J. and Woodard, P. K. (2007): In vivo/ex vivo MRI-based 3D models with fluid-structure interactions for human atherosclerotic plaques compared with fluid/wall-only models, *CMES: Computer Modeling in Engineering and Sciences,* 19(3):233-245.

Yang, C., Tang, D.; Yuan, C., Kerwin, W., Liu, F., Canton, G., Hatsukami, T. S., Atluri, S. (2008): Meshless generalized finite difference method and human carotid atherosclerotic plaque progression simulation using multi-year MRI patient-tracking data, *CMES: Computer Modeling in Engineering and Sciences,* 28(2):95-107.

Young, D. L.; Chen, K. H.; Liu, T. Y.; Shen, L. H.; Wu, C. S. (2009): Hypersingular meshless method for solving 3D potential problems with arbitrary domain, *CMES: Computer Modeling in Engineering & Sciences,* 40(3):225-270

Zhang, Y.; Wang, W.; Liang, X.; Bazilevs, Yuri.; Hsu, M. C.; Kvamsdal, T.;, Brekken, R.; Isaksen. J. (2009): High-fidelity tetrahedral mesh generation from medical imaging data for fluid-structure interaction analysis of cerebral aneurysms, *CMES: Computer Modeling in Engineering & Sciences,* 42(2):131-150.

Zheng, J.; Long, S.; Xiong, Y.; Li, G. (2009): A finite volume meshless local Petrov-Galerkin method for topology optimization design of the continuum structures, *CMES: Computer Modeling in Engineering & Sciences,* 42(1):19-34

Zohouri S.; Pirooz, M. D.; and Esmaeily, A. (2004): Predicting wave run-up using full ALE finite element approach considering moving boundary, *CMES: Computer Modeling in Engineering & Sciences,* 7(1):107-118.